



HAL
open science

CO₂ adsorption in nanosized RHO zeolites with different chemical compositions and crystallite sizes

Giorgia Confalonieri, Julien Grand, Rossella Arletti, Nicolas Barrier, Svetlana Mintova

► **To cite this version:**

Giorgia Confalonieri, Julien Grand, Rossella Arletti, Nicolas Barrier, Svetlana Mintova. CO₂ adsorption in nanosized RHO zeolites with different chemical compositions and crystallite sizes. *Microporous and Mesoporous Materials*, 2020, 306, pp.110394. 10.1016/j.micromeso.2020.110394 . hal-03027913

HAL Id: hal-03027913

<https://normandie-univ.hal.science/hal-03027913>

Submitted on 30 Nov 2020

HAL is a multi-disciplinary open access archive for the deposit and dissemination of scientific research documents, whether they are published or not. The documents may come from teaching and research institutions in France or abroad, or from public or private research centers.

L'archive ouverte pluridisciplinaire **HAL**, est destinée au dépôt et à la diffusion de documents scientifiques de niveau recherche, publiés ou non, émanant des établissements d'enseignement et de recherche français ou étrangers, des laboratoires publics ou privés.

CO₂ adsorption in nanosized RHO zeolites with different chemical compositions and crystallite sizes

Giorgia Confalonieri,^a Julien Grand,^b Rossella Arletti,^{a,*} Nicolas Barrier,^c Svetlana Mintova,^{b,*}

^a *Dipartimento di Scienze Chimiche e Geologiche, Università degli Studi di Modena e Reggio Emilia, Modena, Italy.*

^b *Normandie Université, ENSICAEN, CNRS, Laboratoire Catalyse et Spectrochimie (LCS), 14500 Caen, France.*

^c *Normandie Université, ENSICAEN, UNICAEN, CNRS, CRISMAT, 14500 Caen, France.*

Abstract

In this work, nanosized RHO zeolite samples with different Si/Al ratios were synthesized and tested for CO₂ adsorption by combining *in situ* IR spectroscopy and *in situ* X-ray powder diffraction using synchrotron radiation. The structural changes of the RHO nanosized zeolites subjected to high temperature treatment (350 °C) and CO₂ adsorption (1 and 5 Bars) studied by high-resolution X ray powder diffraction indicated the presence of two phases with different cell parameters in both samples. The combination of the X-ray technique with IR allowed evaluation of the CO₂ adsorption capacity of the samples and their adsorption dynamic. The results indicated that the CO₂ adsorption capacity is mainly related to the sodium content in the nanosized RHO crystals. The adsorption experiments performed showed that 1 bar CO₂ is sufficient to saturate the RHO samples at room temperature, and no change in the CO₂ adsorption capacity at 5 bars was observed.

Keywords: Na-Cs RHO, nanosized, CO₂ adsorption, *in situ* XRD, *in situ* IR spectroscopy

Highlights:

- Two RHO nanosized zeolite samples with different particle sizes and cations content were synthesized.
- The biphasic nature of RHO zeolite upon dehydration and adsorption of CO₂ is due to the presence of mobile inorganic (Na and Cs) cations.
- The content of charge compensating Na cations influences the CO₂ adsorption of RHO.

1. Introduction

The rise of carbon dioxide and of other greenhouse gases in the atmosphere is believed to be one of the major causes of the global warming [1-4]. CO₂ capture in solid systems provide a way to permanently store, easily transport and, possibly, extract if needed. Several materials such as carbon, polymers, salts, zeolites, calcium oxides for CO₂ adsorption, have been tested [5,6]. Zeolites has demonstrated to be excellent candidate for separation of carbon dioxide [7-15] not only because of their high adsorption capacity but also because of their properties *i.e.* crystal size, pore architecture, chemical composition, and nature of extra-framework cations. On the basis of these, there is an increasing demand for porous materials for the separation of natural gas components (*i.e.* mainly CH₄ and CO₂). Flexible small pore zeolites are interesting candidates due to their high sorption capacity and selectivity [16] and many works focused on their characterization and more specifically on finding the relationship between type of framework, structure and sorption properties. Interesting observations come from X-Ray Powder Diffraction (XRPD). Indeed, this technique is particularly useful since it allows to quantify and localize the adsorbed CO₂ molecules into the zeolite porosities using *in situ* approach during the CO₂ adsorption, thus unravelling the relation among adsorption and structural and chemical characteristic of the host material.

For example, the capacity of Na_{12-x}K_x-A was demonstrated to be strongly related to the occupancy of the so-called site I, where CO₂ is absorbed bridging the two cations placed in the neighboring 8-rings [17]. Structural studies on Li⁺, Na⁺, and K-CHA reveal a preferential CO₂ adsorption site, located in the 8-membered ring due to high van der Waals and quadrupole interactions [18]. In the work of Pham and co-workers, a detailed structural description of CO₂ adsorption was given for ZK-5 exchanged with different cations [19]. Independently from the extra framework cations, three sites were recognized for the CO₂ molecules, the first between the flat eight-membered rings, the second in the α -cage and the third in the γ -cage. In particular, in Li⁺- Na⁺- Mg²⁺- ZK-5 zeolites, the XRD analysis showed the formation of metal-CO₂ complexes upon gas pumping, due to a shift of the cations away from the double six-membered rings toward α -cage. As well as in the above reported example, XRPD was also exploited to investigate nanocrystalline FAU zeolites upon CO₂ adsorption [20]. Structural results showed a different amount of adsorbed CO₂ molecules in nanosized Na-Y and Na-X zeolites supported by the *in situ* IR study revealing the different ratio of chemisorbed and physisorbed CO₂ molecules.

Among different zeolites possibly exploitable in the CO₂ adsorption and/or separation, the RHO-type zeolite [8] is of great interest due to the particular 3D structures consisting of cages and small pore openings. Their selectivity comes from their narrow pore sizes and shapes which can be tuned by the introduction of different extra-framework cations such as K⁺, Na⁺, Cs⁺. Indeed, the extra-framework cations selectively block the access of CO₂ molecules to pores and cages of the zeolite [21].

In this work, we tested the CO₂ capture effectiveness of two nanosized RHO samples with a different grain size and Si/Al ratios and thus with a different amount of extra framework cations occupying the cages to evaluate their effect on the sorption properties. The study was carried out combining *in situ* XRPD using synchrotron radiation and *in situ* IR spectroscopy to reveal the nature and the amount of the CO₂ trapped in RHO zeolites at different pressure (1 and 5 Bars CO₂).

2. Experimental section

2.1. Synthesis of RHO type nanosized zeolites

The reagents used for the hydrothermal synthesis of RHO type nanosized zeolites included the following chemicals without further purification: sodium aluminate (53% Al₂O₃ 47% Na₂O by mass, Sigma-Aldrich), colloidal silica LUDOX AS40 (40% by mass in water, Sigma-Aldrich), sodium hydroxide (99%, Sigma-Aldrich) and cesium hydroxide (98%, Alfa-Aesar).

Two initial precursor suspensions were prepared and used for the synthesis of two RHO zeolite samples with different particle sizes and chemical compositions:

RHO-1: 10 SiO₂ : 0.8 Al₂O₃ : 8 Na₂O : 0.58 Cs₂O : 100 H₂O

RHO-2: 10 SiO₂ : 0.8 Al₂O₃ : 6.6 Na₂O : 0.33 Cs₂O : 100 H₂O

The precursor aqueous suspensions were aged on a magnetic stirrer for 14 h at room temperature. Doubly deionized water was used throughout the synthesis and post-synthesis treatments. Syntheses were carried out in 100 cm³ polypropylene bottle (PP bottle) at autogenous pressure without agitation at 90 °C for 1 h. The solid products were separated and recovered by high-speed centrifugation (20000 rpm, 60 min) and purified until the pH of the decanting water was about 7.5.

2.2. General characterization

Scanning Electron Microscopy: The surface features, morphology, homogeneity and size of RHO zeolite nanocrystals were characterized by field-emission scanning electron microscope (SEM) using a MIRA-LMH (TESCAN) fitted with a field emission gun using an accelerating voltage of 30.0 kV. All samples before the SEM characterization were covered with a Pt conductive layer.

Inductively Coupled Plasma Analysis: The chemical composition of the samples was determined by inductively coupled plasma (ICP) optical emission spectroscopy using a Varian ICP-OES 720-ES; the Si/Al ratio of the samples was confirmed by deconvolution of the ^{29}Si solid state MAS NMR signals using DMFIT software.

Thermogravimetry Analysis: Thermogravimetry analyses (TGA) of the samples were carried out on a SETSYS 1750 CS evolution instrument (SETARAM). The samples were heated from 25 °C to 800 °C with a heating ramp of 5 °C /min (air flow rate: 40 mL/min).

X-Ray Powder Diffraction Data Collection and Analysis. Data collection was performed at ID22 beamline, ESRF, Grenoble, France. Diffracted intensity was detected by a bank of nine detectors, each preceded by a Si(111) crystal analyser. The beam wavelength ($\lambda = 0.3544 \text{ \AA}$) was set by a channel-cut Si(111) crystal monochromator. Measurements were performed as follows: i) at room temperature (labelled *sample r.t.*) ii) samples were then carefully dehydrated at 350°C using a gas blower sample-environment for 3 hours and a further collection was performed (labelled *sample 350 °C*). Diffraction patterns are reported in Figure S1 and S2. Data refinements were performed by GSAS-II program [22] using Le Bail method.

2.3 Adsorption of CO₂ in nanosized zeolites

Volumetric Adsorption Analysis: The adsorption of carbon dioxide on the nanosized RHO zeolite samples was measured at 0 °C using a Micrometrics Model ASAP 2020 volumetric adsorption analyzer. Samples were degassed at 250 °C under vacuum for 12 h prior analysis.

Thermogravimetry Analysis: CO₂ adsorption on the nanosized RHO zeolites after activation at 350 °C for 2 h (water desorption) was performed; the RHO zeolites were kept at room temperature under a continuous flow of CO₂ (flow rate: 40 mL/min, 1 bar) for 9 h. The quantity of CO₂ absorbed in the RHO zeolites was determined using the mass increase compared to the total mass of the initial activated samples.

In situ Infrared Spectroscopy: Zeolite self-supported pellets (10 mg.cm⁻²) were prepared, and the transmission IR spectra with a Nicolet Avatar spectrometer were recorded. IR-cell equipped with

a heating device was used to activate the samples prior to the measurements. The cell was connected to a high vacuum line with a reachable pressure of 10^{-10} bar. The sample was activated at 100 °C for 0.5 h followed by heating at 350 °C for 3.0 h. All the above steps were performed under secondary vacuum. The IR spectra were recorded at room temperature, and the IR spectrum recorded in empty transmission cell under secondary vacuum at room temperature was used as a background.

In situ X-Ray Powder Diffraction Data Collection and Analysis: CO₂ adsorption was performed after the dehydration of RHO zeolite samples (see general characterization XRPD section): i) room temperature was restored and CO₂ was pumped at 1 bar using a Gas-handling capillary cell, and data was recorded after 1 hour of pumping (labelled *sample CO₂ 1 bar*) and ii) CO₂ was then pumped at 5 bar and data collection was performed after 1 hour of pumping (labelled *sample CO₂ 5 bar*). Beamline used setup is the same as the reported one for the measurements at room temperature (r.t.) and at 350°C; diffraction patterns are presented in Figure S1 and S2. The acentric space group $I\bar{4}3m$ is the preferred for RHO zeolites with a cell parameter lower than 14.95 Å according to Ref. [23], therefore Le Bail analysis of the RHO samples was performed using acentric space group for both samples.

3. Results & discussions

3.1. Characterization of as-synthesized nanosized RHO zeolite samples

Morphology and porosity.

The SEM images reveal the presence of homogeneous RHO crystals with regular round-shapes in both samples RHO-1 and RHO-2 (Figure 1).

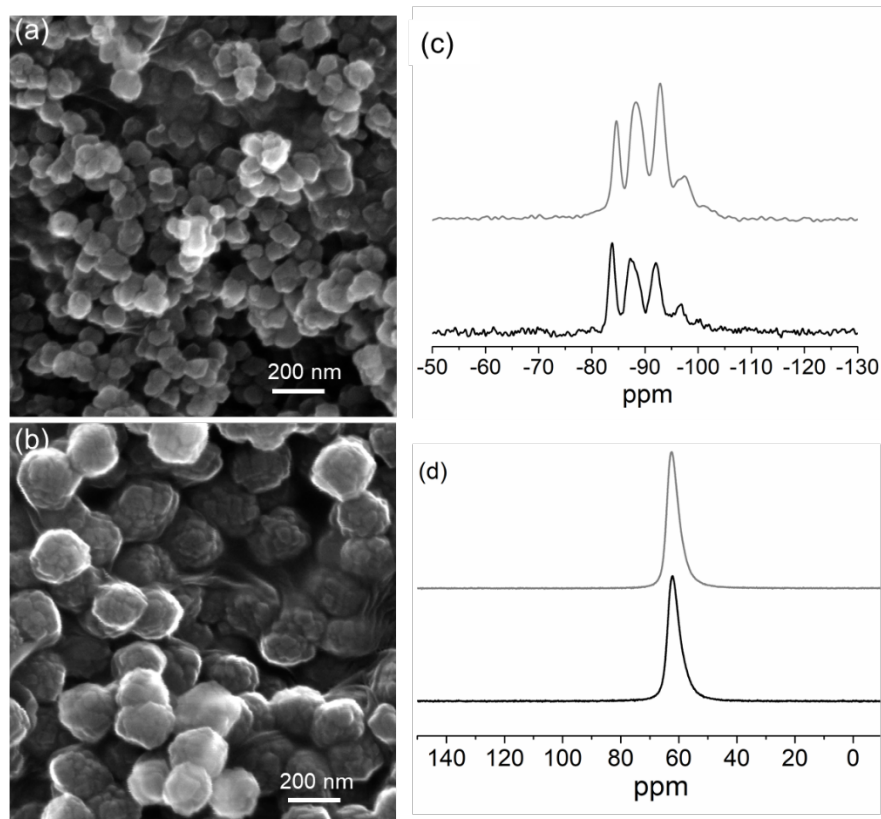


Figure 1. SEM images of (a) RHO-1 and (b) RHO-2 samples and (c) ^{29}Si MAS NMR and (d) ^{27}Al NMR spectra of RHO-1 (black) and RHO-2 (grey) samples.

Indeed, RHO-1 zeolite sample has a particle diameter of around 80 nm while RHO-2 is formed by smaller particles forming aggregates of around 200 nm. The presence of small discrete nanoparticles in sample RHO-1 is further confirmed by the N_2 sorption isotherm revealing the presence of high textural porosity due to the presence of nanosized homogenous crystals (Figure 2). The hysteresis loop above 0.8 P/P_0 in the N_2 sorption isotherm of RHO-1 corresponds to the interparticles mesoporosity, while this is not well-pronounced for sample RHO-2; this is explained with the aggregates having bigger ultimate particle size. The agglomerated RHO-2 crystals do not possess high external surface area nor interparticles mesoporosity as clearly shown by the low intensity of the hysteresis loop above 0.8 P/P_0 . The total pore volume of RHO-1 sample is higher than for RHO-2, and the absence of microporosity for both samples is expected since the pores are blocked with the cations used for the synthesis of the RHO-1 and RHO-2 samples (Figure 2).

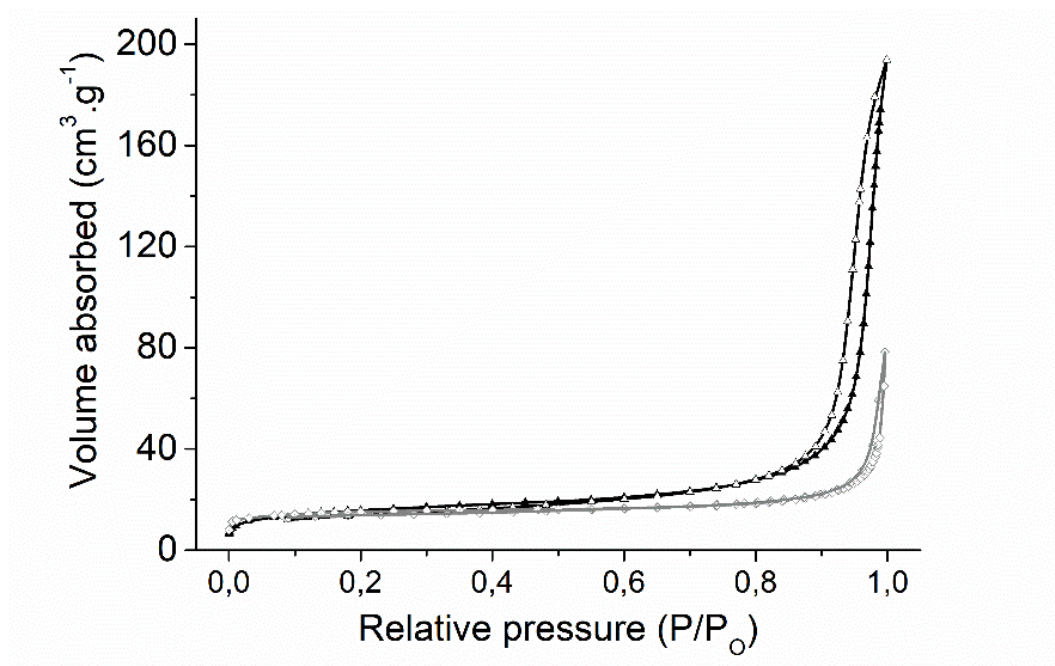


Figure 2. Nitrogen adsorption-desorption isotherms of nanosized RHO-1 (black) and RHO-2 (grey) zeolites (closed symbols: adsorption and open symbols: desorption).

Chemical Composition.

The ICP analysis for samples RHO-1 and RHO-2 reveal the molar Si/Al ratio of 1.46 and 1.71, respectively. More precisely, the overall chemical composition of both samples has been determined based on ICP results:



The ^{29}Si MAS NMR spectra were used to verify the Si/Al ratio of the materials (Figure 1c). Peaks at -84 ppm, -88 ppm, -92 ppm, -98 ppm and -102 ppm correspond to Q^0 (4Al), Q^1 (3Al), Q^2 (2Al), Q^3 (1Al) and Q^4 (0Al) types of silicon in tetrahedral positions. After being normalized with the mass of samples, those peaks have been deconvoluted and their respective areas allowed to calculate the molar Si/Al ratio of 1.55 for RHO-1 and 1.75 for RHO-2. No peak corresponding to octahedral aluminum at 0 ppm in ^{27}Al MAS NMR spectra of both samples was observed, thus confirming that no amorphous alumina was present (Figure 1d).

The RHO-1 material has a lower Si/Al ratio compared to RHO-2, probably due to the highest content of cations in the initial precursor suspension. It is interesting to notice that Cs⁺ cations content is rather similar in both samples. While the Na⁺ content is higher in RHO-1 sample, which is expected since they must compensate the high Al loading.

X-Ray Powder Diffraction Analysis.

Highly crystalline RHO materials were obtained as proved by the two diffraction patterns shown in Figure 3 (top and medium panel). RHO-1 and RHO-2 present two different peak broadening and signal dampening (Figure 3, bottom panel) due to the smaller domain size (*i.e.* crystallite dimension) of the second sample, which is consistent with the SEM analysis. Indeed, as previously reported, the RHO-2 sample consists of aggregates (200 nm) formed by smaller nanocrystallites of about 30-40 nm. Minor impurities were detected in both samples, the presence of only few low intensity peaks did not allow the phase identification.

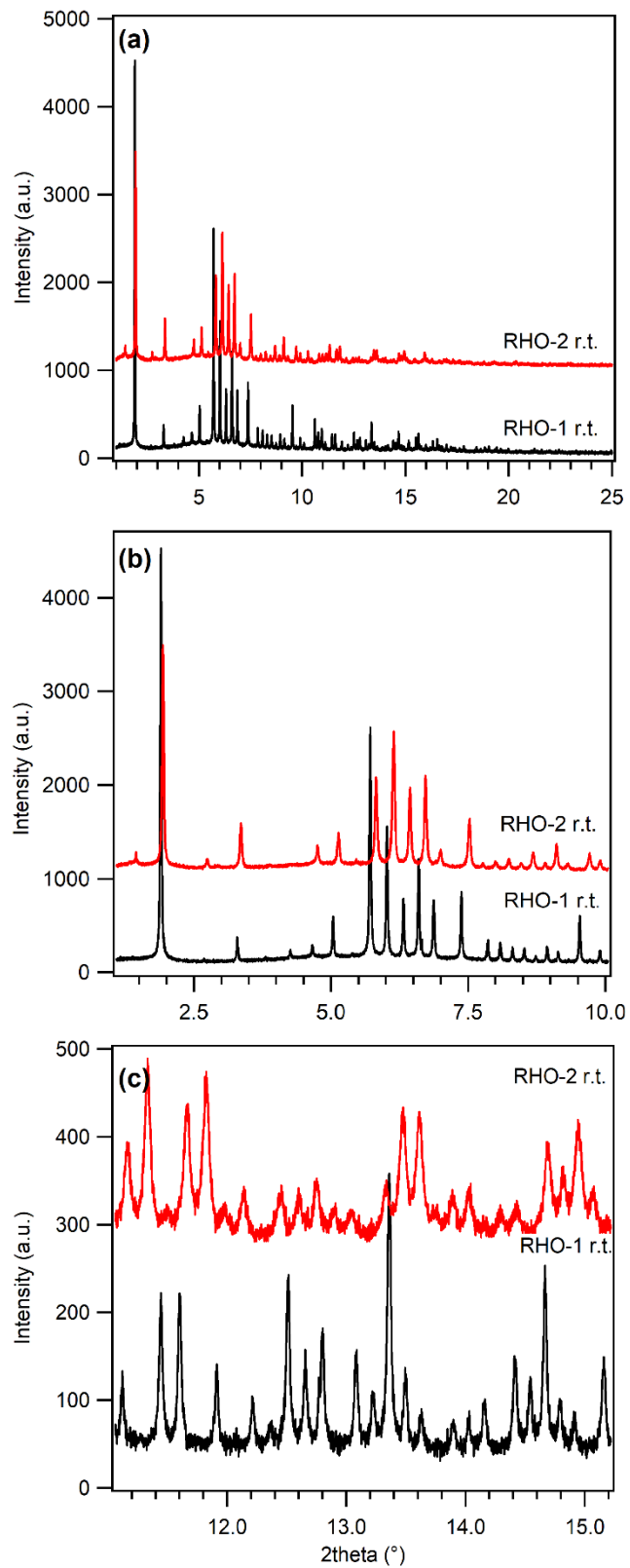


Figure 3. Diffraction patterns of RHO-1 and RHO-2 collected at room temperature before dehydration in the range (a) 1-25 ° 2theta, (b) 2-10 ° 2theta and (c) 11-15 ° 2theta.

3.2. Characterization of dehydrated nanosized RHO zeolite samples

Figure 4 shows the diffraction patterns of RHO-1 and RHO-2 samples after dehydration (see experimental section). After dehydration, the XRPD patterns of both RHO-1 and RHO-2 samples present split peaks indicating the presence of two phases with different cell parameters.

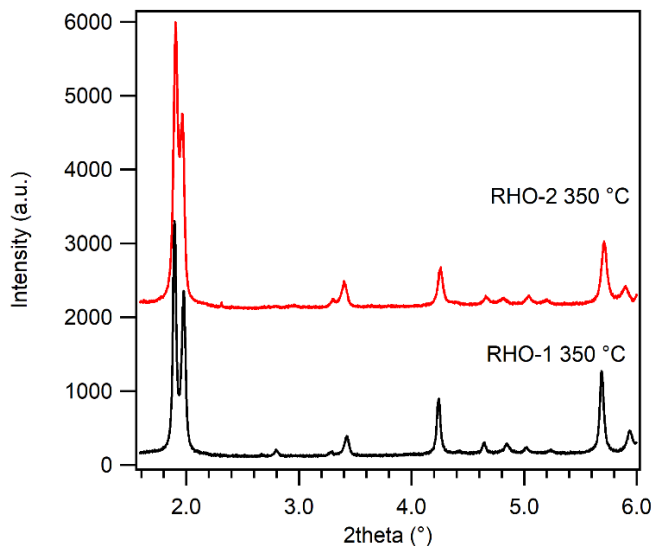


Figure 4. XRPD patterns of nanosized RHO-1 and RHO-2 zeolite samples collected after dehydration at 350 °C.

Parise and co-workers already reported this behaviour in Cd exchanged RHO zeolite [24]. This zeolite, indeed, upon dehydration, presents a transformation from $I\bar{4}3m$ to $Im\bar{3}m$ space group with a displacement of Cd^{2+} ions, initially positioned near to the centre of the single 8-ring (S8R), to the S6R-site. Due to the very slow structural changes, diffraction patterns show two coexisting phases, one acentric and the other centric. In our case, the observations for the nanosized RHO zeolites are different. Indeed, the diffraction pattern collected of sample RHO-1 at room temperature, despite the high peak broadening due to the nanosized crystals dimension, shows slight peak splits and appearance of shoulders originated by a second phase which are identified even at room temperature thanks to the high-resolution data obtained using synchrotron radiation (Figure 5). The two phases, named (*a*) and (*b*), show very similar, but distinct, cell parameters: 15.0813(2) Å and 15.0742(4) Å (see Table 1).

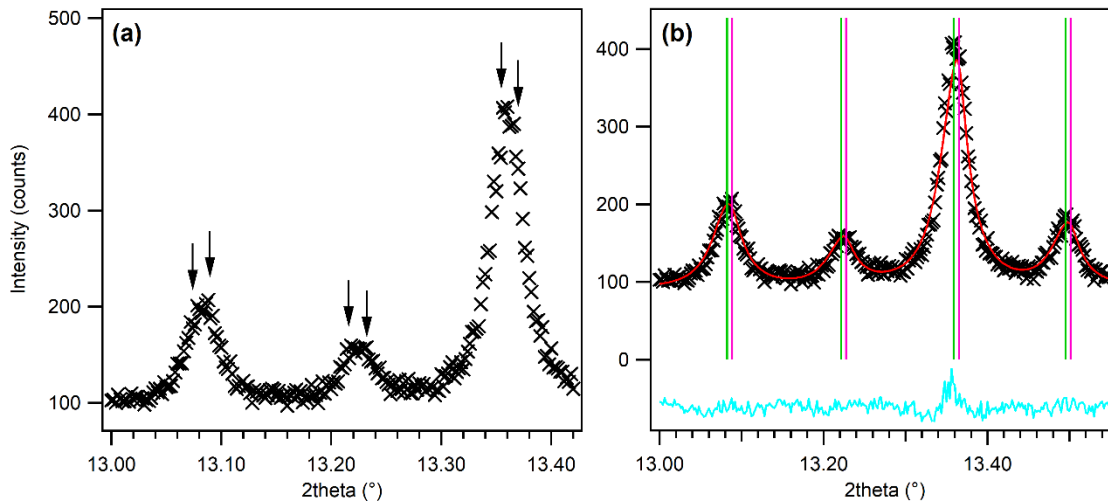


Figure 5. (a) XRD patterns of nanosized RHO-1 zeolite at room temperature (arrows indicate the peak splits due to the presence of a second phase, and (b) the refinement of XRD patterns RHO-1 at room temperature (black cross represents the observed pattern, red line the calculated pattern and cyan line is the differences between the two; green and pink markers are related to the reflections belonging to phase (a) and (b).

No structural refinements can be performed due to the biphasic nature of the sample. We may suppose the presence of two different phases, coexisting at room temperature, also for sample RHO-2, but here the smaller nanosized crystals domains strongly affects the peak broadening, thus no signal of a second phase is clearly recognized. RHO-2 sample present at room temperature an “average” cell parameter of 14.8005(2) Å. Overall, the presence of two different phases is more clearly observed in dehydrated condition. Each sample consists of two phases (a) and (b) characterized by two different cell parameters (Table 1). The two phases depend on the chemical composition of the RHO zeolite, and phases (a) has always the larger cell parameter which is probably due to the larger Al content and higher concentration of extra framework cations (Na and Cs). For sample RHO-1, the dehydration induces a cell parameter decrease for the phase with higher cation contents (a) and a cell parameter increase for the phase with less cations content (b). This different behavior is linked to the different water content in the two phases: in phase (a), where more cations are present (higher Al content in the RHO structure) thus water molecules are hosted, and the thermal behaviour is mostly influenced by water release (i.e. contraction of the cell parameter), while in phase (b) is mostly influenced by the thermal expansion (i.e. expansion of the cell parameter). This is applicable for the RHO-2 sample, but due to the smaller differences between the cell parameter of phase (a) and (b) at dehydrated condition and to the smaller nanosized crystals domains, it is not possible to identify the presence of the two phases at ambient

conditions (RT), since their peaks appear superimposed revealing only an “average” cell parameter.

Table 1. Cell parameters obtained after refinement for RHO-1 and RHO-2 samples.

	RHO-1		RHO-2	
	Phase (a) (Å)	Phase (b) (Å)	Phase (a) (Å)	Phase (b) (Å)
r.t.	15.0813(2)	15.0742(4)	14.8005(2)	
350 °C	14.526(1)	15.1460(4)	14.620(2)	15.0839(7)
1 bar	14.3590(6)	14.551(1)	14.505(2)	14.6690(8)
5 bar	14.3706(8)	14.549(1)	14.502(1)	14.7031(8)

Besides the different amount of water molecules in the two hydrated phases at r.t., other factor could be co-responsible of the variations of the unit cell such as: i) possible phase transition of one of the two phases [24], ii) different cations contents with different cesium displacement, and iii) a combination of the previous two hypotheses.

3.3. CO₂ adsorption on dehydrated nanosized RHO zeolite samples

BET and TGA analyses

The CO₂ adsorption on dehydrated RHO-1 and RHO-2 samples was followed by BET and TGA methods (Figure 6). Each of the two zeolites is consisting of two slightly different phases, as indicated by XRPD analysis (see section above), however, the BET and TGA results represent the average behavior of samples.

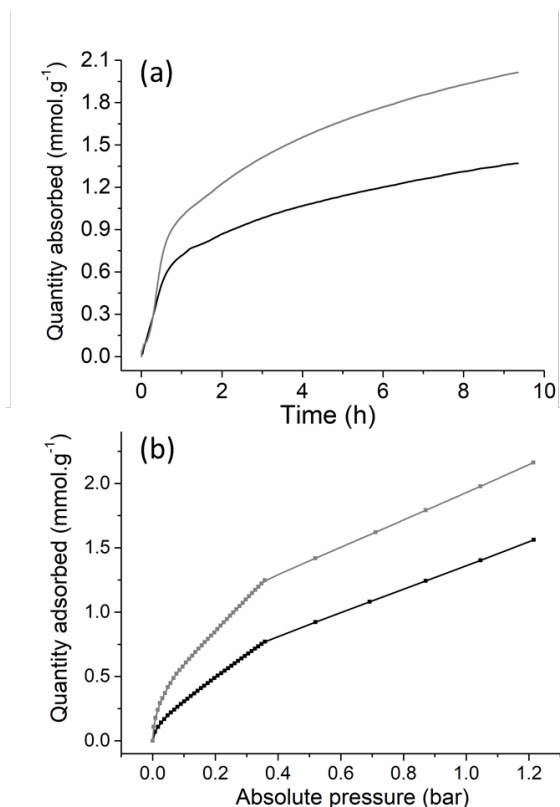


Figure 6. CO₂ adsorption monitored on nanosized RHO-1 (black) and RHO-2 (grey) zeolite samples by (a) TGA and (b) BET at 0 °C (details are presented in the Experimental section).

The same trend on both samples at the initial stages of CO₂ adsorption at 1 bar is observed (Figure 6a). The total adsorption of CO₂ on RHO-1 and RHO-2 after 9 h reached is 1.3 and 2 mmol g⁻¹, respectively as measured by TGA. The isotherms collected at 0 °C confirmed this tendency that the RHO-2 sample has a higher capacity for CO₂ than the RHO-1, but the trend in the adsorption is similar (Figure 6b). The different CO₂ capacity of the two samples is probably due to the different cation contents in the RHO framework. The more Na⁺ cations are present in the RHO type framework, the lower the capacity of the RHO zeolite towards CO₂ is measured. As the Cs⁺ cation contents in both samples are similar, the trends of adsorption observed in TGA and BET isotherms are rather similar. Cs⁺ cations are responsible for the selective adsorption of CO₂ and possible rejection of bulky molecules such as CH₄ [25].

In situ FTIR analysis.

In order to understand the type of CO₂ species adsorbed in the samples, *in situ* FTIR study on both nanosized RHO-1 and RHO-2 zeolite samples was carried out. CO₂ gas with small doses from 1 to 760 T was delivered to the activated self-supported zeolite pellet (Figure S3 and S4). As shown in both sets of the IR spectra, water was present confirmed by the peak at 1610 cm⁻¹. The intensity of this peak corresponding to water is gradually increased with an increase of CO₂ concentration. The CO₂ absorption in the RHO zeolite is confirmed by the presence of a band at 2250 cm⁻¹ corresponding to physisorbed CO₂ as well several bands around 1650 cm⁻¹ due to the chemisorbed CO₂ species. The chemisorbed CO₂ is originated from the formation of carbonates in the presence of water. The *in situ* IR results show that RHO-2 has higher CO₂ capacity, which is due to the lower concentration of Na cations in the sample (Figure S5). These results are in a good accordance with the BET and TGA data shown in the previous section. The high content of Na in the RHO-1 sample leads to a reduced CO₂ capacity.

- *In situ X-Ray Powder Diffraction Analysis.*

The presence of two distinct phases (*a*) and (*b*) in both nanosized RHO-1 and RHO-2 zeolite samples persists after restoring the room temperature conditions and CO₂ pumping. Figure 7 shows the evolution of cell parameters before and during CO₂ adsorption in both zeolite samples (absolute values are reported in Table 1). In both samples phases (*a*) and (*b*) experience a reduction of the cell parameters due to the penetration of CO₂ molecules at 1 bar in the RHO framework. This behavior was already observed by Polisi et al. [20] where the penetration of molecules into the zeolite induced a decrease of the cell volume due to the strong interaction occurring between the framework and the gas molecules. In our case it is not possible to propose further hypothesis to explain this behavior due to the lack of structural information. Nevertheless, we can confirm the CO₂ molecules intrusion in the nanosized RHO-2 zeolite on the basis of the changes in the intensity ratio of diffraction peaks before and after the CO₂ pumping (Figure 8). Under delivering of CO₂ at 5 bars, very little changes in the cell parameters of RHO-1 and 2RHO-2 are observed with respect to that at 1 bar. This indicates the complete saturation of both zeolite sample under CO₂ even at 1 bar.

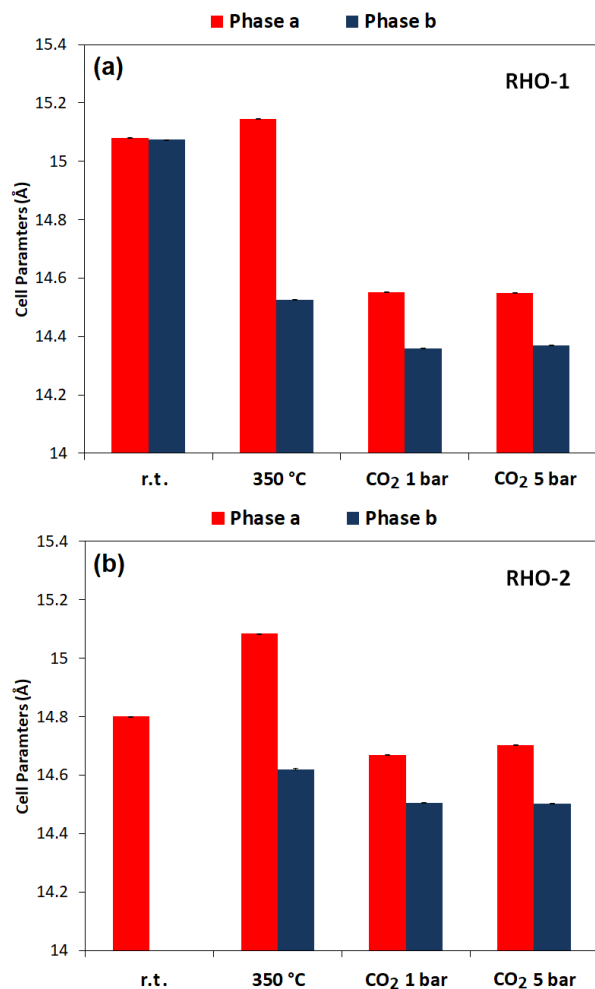


Figure 7. Change of the cell parameters of nanosized RHO-1 and RHO-2 zeolite samples at room temperature (r.t.), after dehydration at 350 °C (a) and under CO₂ adsorption at 1 bar and 5 bars (b).

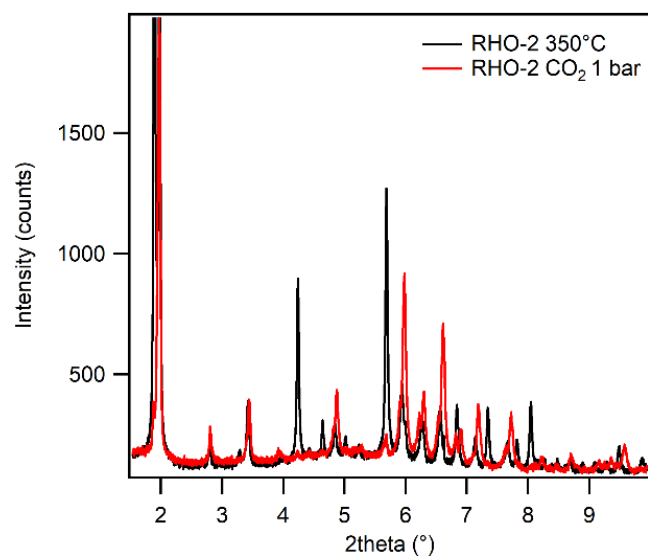


Figure 8. XRD patterns of nanosized RHO-2 zeolite after dehydration at 350 °C and CO₂ adsorption at 1 bar.

4. Conclusions

In this work two different nanosized RHO zeolite samples were synthesized and tested for CO₂ adsorption. Initial materials were fully characterized providing information about chemical composition, morphology and porosity. The two RHO zeolite samples were proved to be highly crystalline, presenting individual grain size of 80 nm for sample RHO-1 and aggregates of 200 nm for sample RHO-2. Upon dehydration, the splitting of the diffraction peaks indicates the presence of two phases with different cell parameters in both samples. Differently from previous works, which report a slow phase transition leading to a biphasic sample, here we observed for the first time, thanks to high resolution XRPD data, the presence of a second phase even at room temperature, probably due to chemical gradients in the samples.

The CO₂ adsorption capacity of the RHO zeolite is controlled by the sodium content in the nanosized crystals with different Si/Al ratios. The Na content can be tuned by modifying the synthesis conditions and this will influence the particle sizes and CO₂ capacity of the RHO materials. Higher Na content in the initial gel is required in order to synthesize pure highly crystalline discrete RHO zeolite by omitting completely the organic structural directing agent.

Acknowledgement

This paper is dedicated to our esteemed colleague and friend Dr. V. Valtchev.

We thank the staff of ID22, ESRF (Grenoble), for the support in the XRPD data collection.

References

- [1] U. Siegenthaler, H. Oeschger, *Tellus B*, 39B (1987) 140-154.
- [2] C.D. Keeling, T.P. Whorf, M. Wahlen, J. van der Plichtt, *Nature*, 375 (1995) 666-670.
- [3] T.R. Anderson, E. Hawkins, P.D. Jones, *Endavour*, 40 (2016) 178-187.
- [4] J.E. Szulejko, P. Kumar, A. Deep, K.H. Kim, *Atmos. Pollut. Res.*, 8 (2017) 136-140.
- [5] R.E. Morris, P.S. Wheatley, *Angew. Chem. Int. Ed.*, 47 (2008) 4966-4981.
- [6] S. Choi, J.H. Drese, C.W. Jones, *Chemsuschem*, 2 (2009) 796-854.
- [7] A. Zukal, J. Mayerova, M. Kubu, *Top. Catal.*, 53 (2010) 1361-1366.
- [8] C. Baerlocher, L.B. McCusker, D.H. Olson, *Atlas of zeolite framework types*, 6th ed., Elsevier, Amsterdam, The Netherlands, 2007.

- [9] J.-S. Lee, J.-H. Kim, J.-T. Kim, J.-K. Suh, J.-M. Lee, C.-H. Lee, *J. Chem. Eng. Data*, 47 (2002) 1237-1242.
- [10] C.Y. Lu, H.L. Bai, B.L. Wu, F.S. Su, J. Fen-Hwang, *Energy & Fuels*, 22 (2008) 3050-3056.
- [11] R.V. Siriwardane, M.S. Shen, E.P. Fisher, *Energ. Fuels*, 19 (2005) 1153-1159.
- [12] G. Maurin, P.L. Llewellyn, R.G. Bell, *J. Phys. Chem. B*, 109 (2005) 16084-16091.
- [13] D.F. Plant, G. Maurin, I. Deroche, P.L. Llewellyn, *Microporous and Mesoporous Mater.*, 99 (2007) 70-78.
- [14] W. Wong-Ng, J.A. Kaduk, Q. Huang, L. Espinal, L. Li, J.W. Burrell, *Microporous and Mesoporous Mater.*, 172 (2013) 95-104.
- [15] R. Arletti, L. Gigli, F. di Renzo, S. Quartieri, *Microporous and Mesoporous Mater.*, 228 (2016) 248-255.
- [16] B. Ilic, S.G. Wettstein, *Microporous and Mesoporous Mater.*, 239 (2017) 221-234.
- [17] P. Rzepka, Z. Bacsik, S. Smeets, T.C. Hansen, N. Hedin, D. Wardecki, *J. Phys. Chem. C*, 122 (2018) 27005-27015.
- [18] T.D. Pham, M.R. Hudson, C.M. Brown, R.F. Lobo, *Chemsuschem*, 7 (2014) 3031-3038.
- [19] T.D. Pham, M.R. Hudson, C.M. Brown, R.F. Lobo, *Chemsuschem*, 10 (2017) 946-957.
- [20] M. Polisi, J. Grand, R. Arletti, N. Barrier, S. Komaty, M. Zaarour, S. Mintova, G. Vezzalini, *J. Phys. Chem. C*, 123 (2019) 2361-2369.
- [21] T. De Baerdemaeker, D. De Vos, *Nature Chemistry*, 5 (2013) 89-90.
- [22] B.H. Toby, R.B. Von Dreele, *J. Appl. Crystallogr.*, 46 (2013) 544-549.
- [23] J.B. Parise, T.E. Gier, D.R. Corbin, *J. Phys. Chem.*, 88 (1984) 1635-1640.
- [24] J.B. Parise, L. Xing, D.R. Corbin, *J. Chem. Soc. Chem. Comm.*, (1991) 162-163.
- [25] F.X. Coudert, D. Kohen, *Chem. Mater.*, 29 (2017) 2724-2730.